ARTICLE IN PRESS

Available online at www.sciencedirect.com

ScienceDirect

ELSEVIER

Planetary and Space Science ▮ (▮▮▮▮) ▮▮▮–▮▮▮

Planetary and Space Science

www.elsevier.com/locate/pss

Correlations between Cassini VIMS spectra and RADAR SAR images: Implications for Titan's surface composition and the character of the Huygens Probe Landing Site

Laurence A. Soderblom[a,*], Randolph L. Kirk[a], Jonathan I. Lunine[b], Jeffrey A. Anderson[a], Kevin H. Baines[c], Jason W. Barnes[b,d], Janet M. Barrett[a], Robert H. Brown[b], Bonnie J. Buratti[c], Roger N. Clark[e], Dale P. Cruikshank[d], Charles Elachi[c], Michael A. Janssen[c], Ralf Jaumann[f], Erich Karkoschka[b], Stéphane Le Mouélic[g], Rosaly M. Lopes[c], Ralph D. Lorenz[h], Thomas B. McCord[i], Philip D. Nicholson[j], Jani Radebaugh[k], Bashar Rizk[b], Christophe Sotin[g], Ellen R. Stofan[l], Tracie L. Sucharski[a], Martin G. Tomasko[b], Stephen D. Wall[c]

[a] *US Geological Survey, Flagstaff, AZ, USA*
[b] *Lunar and Planetary Laboratory, University of Arizona, Tucson, AZ, USA*
[c] *Jet Propulsion Laboratory, California Institute of Technology, Pasadena, CA, USA*
[d] *NASA AMES Research Center, Moffett Field, CA, USA*
[e] *US Geological Survey, Denver, CO, USA*
[f] *DLR Institute for Planetary Exploration, Berlin, Germany*
[g] *University of Nantes, Nantes, France*
[h] *Applied Physics Laboratory, Johns Hopkins University, Laurel, MD, USA*
[i] *HIGP/SOEST, University of Hawaii, HI, USA*
[j] *Cornell University, Ithaca, NY, USA*
[k] *Brigham Young University, Provo, UT, USA*
[l] *Proxemy Research, Rectortown, VA, USA*

Accepted 13 April 2007

Abstract

Titan's vast equatorial fields of RADAR-dark longitudinal dunes seen in Cassini RADAR synthetic aperture images correlate with one of two dark surface units discriminated as "brown" and "blue" in Visible and Infrared Mapping Spectrometer (VIMS) color composites of short-wavelength infrared spectral cubes (RGB as 2.0, 1.6, 1.3 μm). In such composites bluer materials exhibit higher reflectance at 1.3 μm and lower at 1.6 and 2.0 μm. The dark brown unit is highly correlated with the RADAR-dark dunes. The dark brown unit shows less evidence of water ice suggesting that the saltating grains of the dunes are largely composed of hydrocarbons and/or nitriles. In general, the bright units also show less evidence of absorption due to water ice and are inferred to consist of deposits of bright fine precipitating tholin aerosol dust. Some set of chemical/mechanical processes may be converting the bright fine-grained aerosol deposits into the dark saltating hydrocarbon and/or nitrile grains. Alternatively the dark dune materials may be derived from a different type of air aerosol photochemical product than are the bright materials. In our model, both the bright aerosol and dark hydrocarbon dune deposits mantle the VIMS dark blue water ice-rich substrate. We postulate that the bright mantles are effectively invisible (transparent) in RADAR synthetic aperture radar (SAR) images leading to lack of correlation in the RADAR images with optically bright mantling units. RADAR images mostly show only dark dunes and the water ice substrate that varies in roughness, fracturing, and porosity. If the rate of deposition of bright aerosol is ~0.1 μm/yr, the surface would be coated (to optical instruments) in a few years

*Corresponding author. Tel.: +1 928 556 7018; fax: +1 928 556 7014.
E-mail address: lsoderblom@usgs.gov (L.A. Soderblom).

0032-0633/$ - see front matter
doi:10.1016/j.pss.2007.04.014

Please cite this article as: Soderblom, L.A., et al., Correlations between Cassini VIMS spectra and RADAR SAR images: Implications for Titan's surface composition and the character of the Huygens Probe Landing Site, Planet. Space Sci. (2007), doi:10.1016/j.pss.2007.04.014

unless cleansing processes are active. The dark dunes must be mobile on this very short timescale to prevent the accumulation of bright coatings. Huygens landed in a region of the VIMS bright and dark blue materials and about 30 km south of the nearest occurrence of dunes visible in the RADAR SAR images. Fluvial/pluvial processes, every few years-to-decades, must be cleansing the dark floors of the incised channels and scouring the dark plains at the Huygens landing site both imaged by Descent Imager/Spectral Radiometer (DISR).

Keywords: Titan; VIMS; Radar; SAR; DISR; Dunes; Mantles; Coatings; Substrate; Water ice; Hydrocarbons; Titriles; Tholin; Aerosols

1. Background

In exploring the surface of Titan, an extremely powerful combination of data from the Cassini Orbiter instruments is joint coverage by the multi-mode RADAR Investigation and the Visible and Infrared Mapping Spectrometer (VIMS). The RADAR operates at K_u-band (13.78 GHz frequency or 2.17 cm wavelength) and collects low-resolution (several to tens of km) scatterometer, altimeter, and radiometer data as well as very high-resolution (~350 m) synthetic aperture radar (SAR) images covering large strips of Titan's surface (Elachi et al., 2004). VIMS collects spectral cubes that are more limited in spatial coverage, the best usually a few km in resolution (and rarely a few hundred meters in resolution), but covers a large spectral range from 0.35 to 5.2 μm (Brown et al., 2004). A principal focus of this paper is the correlation of images and maps of Titan's surface acquired by the RADAR in SAR mode and by VIMS through the CH_4 windows in Titan's atmosphere centered near 1.3, 1.6, and 2.0 μm. Once established, these correlations are used to infer the character and composition of Titan's surface in general and of the Huygens landing site, in particular, and to further correlate these observations with the visible-light images acquired by DISR (the Descent Imager/Spectral Radiometer) during the descent of the Huygens Probe (Tomasko et al., 2002).

This paper is as much about what does not as what does correlate between the RADAR, VIMS, and DISR images. By way of background it is useful to review the coverage of Huygens Probe landing site (HLS) by these instruments (Fig. 1). During Titan pass T_a on October 26, 2004, a VIMS spectral cube was acquired with a resolution of ~15 km/pixel. The predicted location of the HLS in the VIMS image was uncertain by 50–100 km, a substantial error, as can be gauged by the scale bar in Fig. 1. The best guess was that the probe would land in a region of mixed bright and dark materials. Huygens descended to the surface on January 14, 2005; the DISR images showed the HLS to be a few km south of a bright-dark boundary in a dark plain laced with bright units (Tomasko et al., 2005). The large disparity in resolution and difference in wavelength between VIMS and DISR coupled with HLS positional and VIMS pointing uncertainties made locating HLS in VIMS, at that time, impossible.

On October 28, 2005 the Cassini RADAR collected high-resolution SAR images of the HLS region on Titan pass T_8 (Lunine et al., submitted). Because the SAR images are constructed from range and Doppler information, rather than from geometric pointing as are optical instruments, the positional errors in the SAR images are of the order of the errors in the trajectory that when refined result in map errors <10 km. So the task of finding the HLS location using the RADAR images and thereby locating the HLS in the VIMS image, was expected to be quite straightforward. However when the three data sets were first compared they bore little resemblance to each other. The western halves of the VIMS and SAR images shown in Fig. 1 are remarkable in the *absence* of any obvious correlation among surface features. By marked contrast, the eastern halves of the images do show several

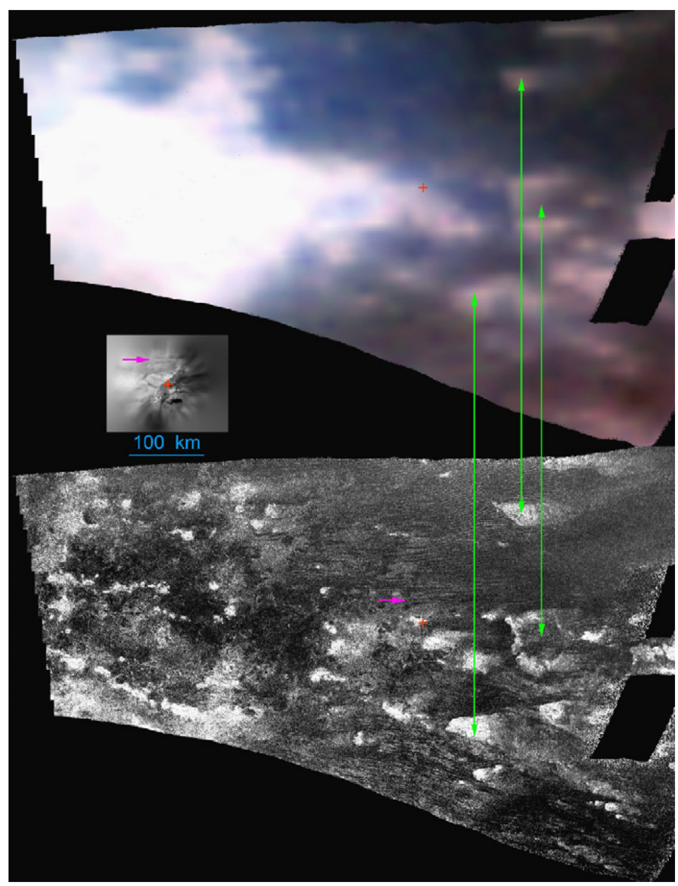

Fig. 1. VIMS, DISR, and RADAR coverage of the region of the Huygens landing site, all to the same scale. *Top:* VIMS image from pass T_a (CM_1477491859; RGB≡2.0, 1.6, 1.3 μm); *Middle:* Mosaic of all DISR visible-camera images showing surface features (Karkoschka, 2006); *Bottom:* SAR image from Titan pass T_8. The red "+" in each marks the current best estimate of the HLS (10.4°S, 192.4°W). Green arrows show correlatable features. VIMS and RADAR images have been stenciled to show only common coverage. Magenta arrows denote a pair of longitudinal dunes visible in both DISR and SAR images. Projections are simple cylindrical.

Please cite this article as: Soderblom, L.A., et al., Correlations between Cassini VIMS spectra and RADAR SAR images: Implications for Titan's surface composition and the character of the Huygens Probe Landing Site, Planet. Space Sci. (2007), doi:10.1016/j.pss.2007.04.014

correlated features (green arrows). One of the key subjects of this paper is to show that these correlations arise largely from the presence of vast "seas" of longitudinal dunes discovered in the Cassini SAR images (Lorenz et al., 2006). These dune materials are one of the few materials that appear to be distinguishable in images returned by all three instruments. In fact Lunine et al. (submitted) show that a pair of isolated, parallel E–W dunes that can clearly be seen in both DISR and SAR images (denoted by magenta arrows in Fig. 1) are among the few features that allow us to tie down the location of the HLS in the SAR image, as of now with an accuracy of ~5 km. The purpose of this paper is to explore the spectral properties of the dune and non-dune areas, to hypothesize differences in composition, and to apply these observations to characterize the properties of the immediate region of the Huygens landing site and of Titan's surface in general.

2. VIMS surface units mapped in the 1–2 μm spectral region

Although the VIMS spectral range is 0.35–5.2 μm, the spectral region in which the surface can be imaged with any clarity is far more restricted. Fig. 2 shows typical VIMS spectra of bright and dark areas (location shown in Fig. 3) that were selected so as to have the same incidence and emission angles and thus similar contributions of scattering haze. The prominent features in the spectra are the deep absorption bands and atmospheric windows due mostly to CH_4. Due to the optically thick scattering haze particles, below ~1 μm in the visible region, the contrast nearly vanishes. From DISR images acquired within a few km of the surface we know that the contrast at the surface in the visible is about 2:1 (Tomasko et al., 2005); so the lack of contrast in the VIMS spectra is due to strong multiple scattering by aerosol particles. At longer wavelengths, beyond ~1 μm, the contrast rapidly increases as the aerosol scattering drops off. Here, the signal-to-noise ratio (SNR) is high and surface contrast is quite strong in the 1.3, 1.6,

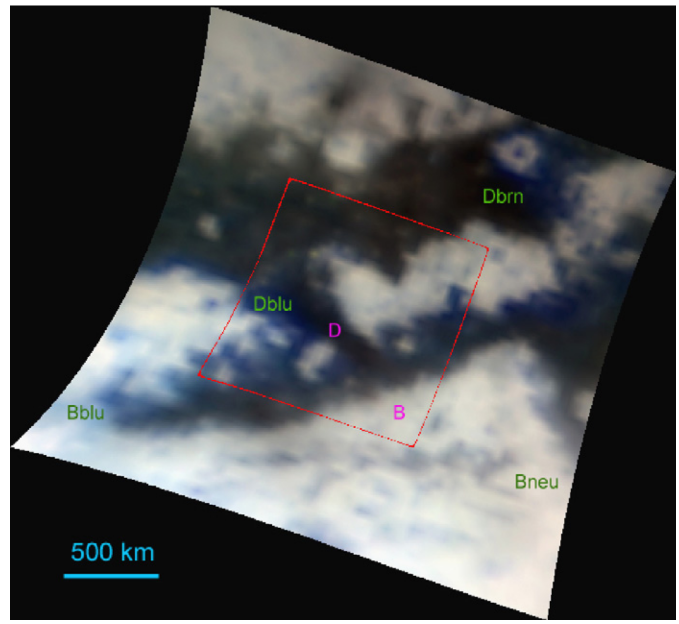

Fig. 3. VIMS color composite of Quivira and surrounding regions made from spectral images in three methane windows: blue = 1.3 μm, green = 1.6 μm, red = 2.0 μm for cube CM_1514302573. Projection is simple cylindrical. Magenta symbols locate two spectra shown in Fig. 2; green symbols (Bblu = bright blue, Bneu = bright neutral, Dblu = dark blue, Dbrn = dark brown) locate spectra in Fig. 4; outline of the area of for cluster analysis in Fig. 5 is in red. Central latitude/longitude is ~7°S, 36°W.

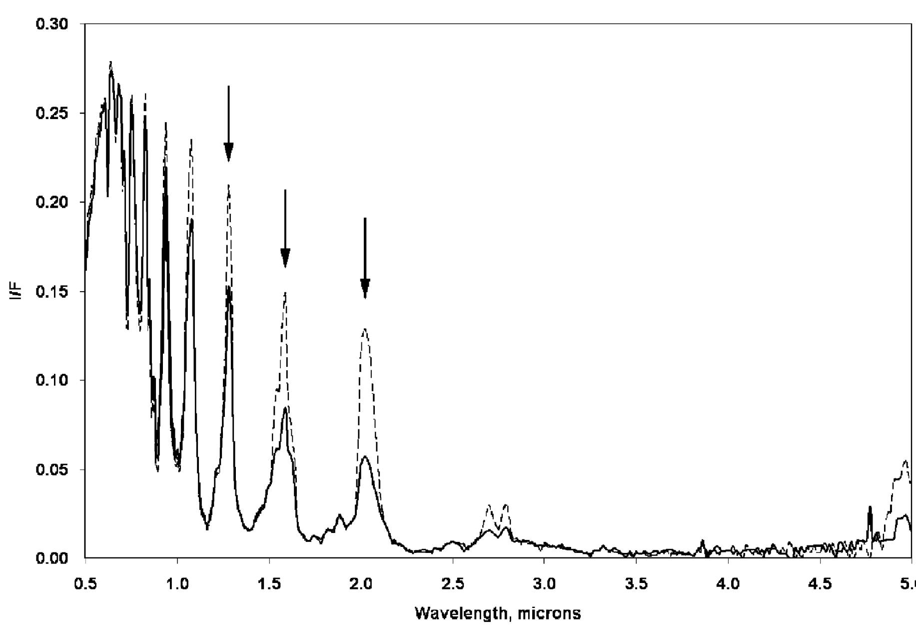

Fig. 2. Comparison of VIMS spectra for brightest and darkest units: bright (dashed) and dark (solid) units chosen to have the same incidence (10°) and emission (20°) angles. The locations of the bright (B) and dark (D) spectra are shown by magenta symbols in Fig. 3. Arrows indicate the CH_4 windows selected for mapping the surface composition in this work. I/F is the observed spectral radiance divided by the solar irradiance.

Please cite this article as: Soderblom, L.A., et al., Correlations between Cassini VIMS spectra and RADAR SAR images: Implications for Titan's surface composition and the character of the Huygens Probe Landing Site, Planet. Space Sci. (2007), doi:10.1016/j.pss.2007.04.014

and 2.0 μm windows. The VIMS surface signal again becomes very weak beyond ~2 μm as the solar flux falls off and the surface albedo itself may also drop rapidly, particularly in the 2.5–3.0 μm region (Coustenis et al., 2006). For these reasons in the present work we restrict surface mapping to the 1.3–2.0 μm region. Others have attempted to explore spectral properties of the surface in the lower SNR 2.5–5.2 μm region (Griffith et al., 2003; Lellouch et al., 2004; Coustenis et al., 2006; McCord et al., 2006; Clark et al., 2006).

Fig. 3 illustrates the superb quality of VIMS surface images that can be achieved through the three CH_4 windows noted by arrows in Fig. 2. The region covered is ~3000 km wide centered just east of the prominent bright region, Xanadu. For each window several VIMS channels were averaged: two from 1.270 to 1.303 μm, four from 1.549 to 1.639 μm, and five from 1.994 to 2.076 μm. This image cube was acquired on pass T_9 on December 26, 2005; incidence and emission angles vary between 0°–50° and 0°–55°, respectively. Spectra were selected for four areas (denoted by the green symbols in Fig. 3) to show the full range of spectral variation in this cube; spectra for these four areas are shown in Fig. 4 along with example spectra of water ice for comparison.

Previous studies have shown that spectral properties of dark equatorial regions are consistent with dirty water ice and that bright units appear to have lower concentrations of water ice (Coustenis et al., 1995, 2005; Griffith et al., 2003; McCord et al., 2006; de Pater et al., 2006; Negrão et al., 2006, 2007; Hirtzig et al., 2007). This interpretation is also consistent with DISR near-infrared spectra of the dark plain where Huygens landed that exhibits an absorption feature at 1.5 μm attributable to water ice (Tomasko et al., 2005). Rodriguez et al. (2006) show the VIMS coverage of the HLS is also consistent with local enrichment of exposed water ice. In this work we add that the dark units themselves (and to some degree, bright units) can be further subdivided into those that appear more and less water ice rich. As originally pointed out by Coustenis et al. (1995), it is clear from Fig. 4 that strong water ice absorptions near 1.5 and 2.0 μm bands would significantly affect the surface reflectance as observed through methane windows at 1.6 and 2.0 μm. Note that the reversal in contrast between the VIMS dark blue and dark brown units between the 1.3 and 2.0 μm windows cannot be an atmospheric effect but must arise from spectral reflectance variations of the surface. The dark brown unit is more spectrally neutral than the dark blue unit that shows greater absorption at 1.6 and 2.0 μm. The simplest interpretation is that this arises from greater absorption due to water ice in the dark blue unit relative to the dark brown unit. Clark et al. (2006) caution that a variety of potential hydrocarbons exhibit absorptions that could explain these spectral variations as well. In order to pursue these relationships further, Fig. 5 shows a simple 3-D cluster for a limited region in Fig. 3 (outlined in red) chosen to have limited variance: in incidence angle $<25°$, in emission angle $<35°$, and in phase angle ($25° \pm 0.5°$).

The left panel in Fig. 5 shows how remarkably flat, or two-dimensional, the cluster is. One interpretation is that this flatness arises from three end members that form a simple mixing plane. If water ice is one end member, it would most strongly control the positions in the cluster along the x and y axes; the addition of water ice would

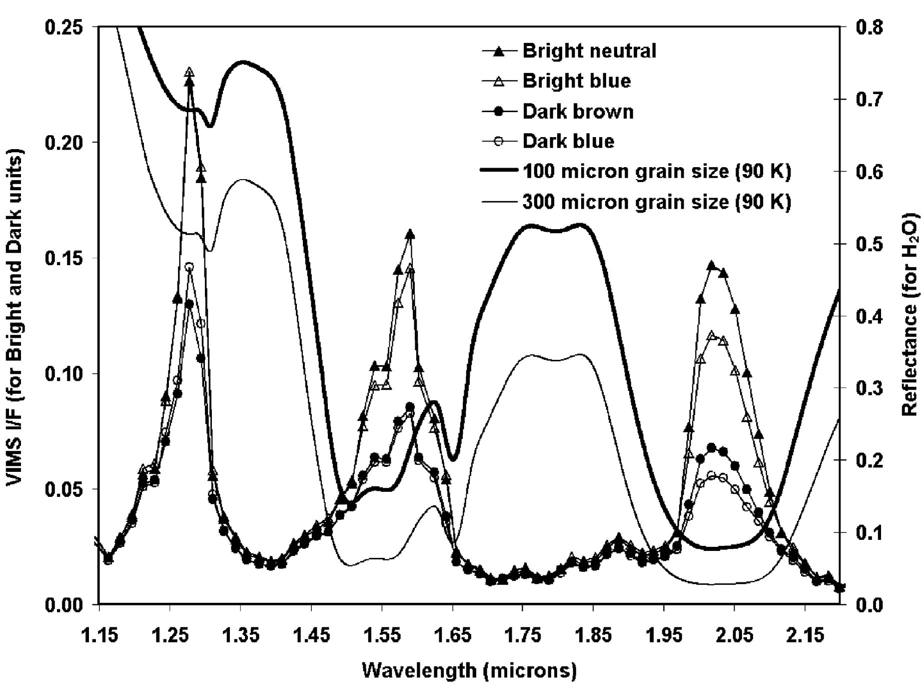

Fig. 4. Spectral variations among the four surface regions denoted in Fig. 3. Also shown are representative spectra of water ice derived from optical constants of Grundy and Schmitt (1998). I/F(λ) is the observed spectral radiance divided by the solar irradiance.

Please cite this article as: Soderblom, L.A., et al., Correlations between Cassini VIMS spectra and RADAR SAR images: Implications for Titan's surface composition and the character of the Huygens Probe Landing Site, Planet. Space Sci. (2007), doi:10.1016/j.pss.2007.04.014

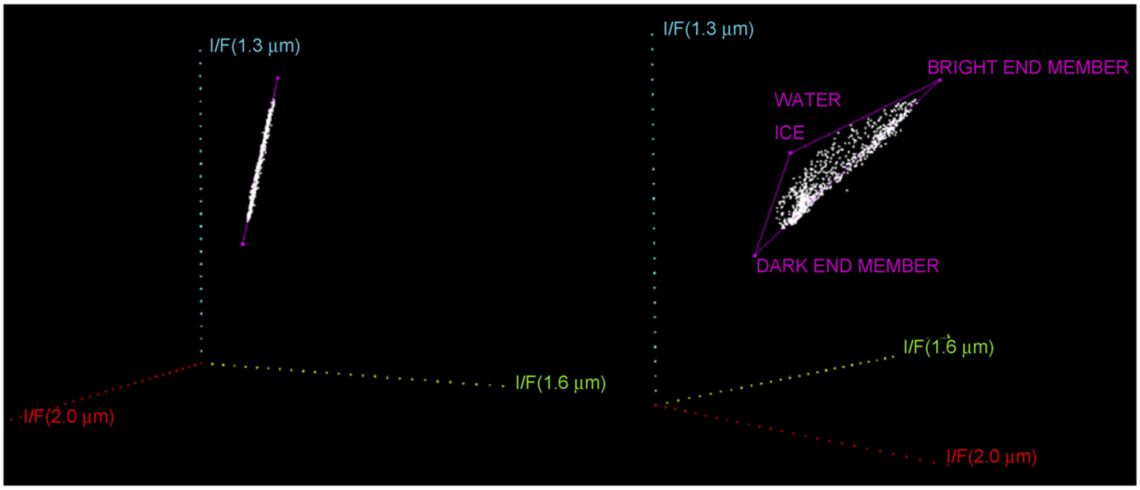

Fig. 5. Perspective views of 3-D cluster for the red-outlined region shown in Fig. 3. The scale for each of the axes ranges from $I/F(\lambda) = 0.0$ to 0.25, where $I/F(\lambda)$ is the observed spectral radiance divided by the solar irradiance.

deflect points in the cluster toward the *z*-axis. The least water ice-rich part of the cluster would then be that part farthest from the *z*-axis. As can be seen in the right panel of Fig. 5 there appears to be a linear distribution of points along this edge, the ends of which we have labeled "bright end member" and "dark end member." This flat cluster was decomposed into the coordinates of the ternary diagram labeled in the right panel of Fig. 5; the position of the apex for "water ice" is somewhat arbitrary. Fig. 6 is a color composite map in which RGB were assigned to each of these ternary components. Although dark units exhibit the greatest variance in mapped water ice enrichment, the bright units do show some variation as well. However, most of the bright material is less water ice rich, consistent with previous work (Griffith et al., 2003; Coustenis et al., 2005; McCord et al., 2006; de Pater et al., 2006; Negrão et al., 2006; Hirtzig et al., 2007). Note that at least in the region studied here, the putative water ice-enriched units (light blue and dark blue) almost always occur in the transition zone between the bright and the dark water-poor units (green and red). After we explore correlations of the VIMS-defined units with RADAR SAR images, we will return to speculations as to what the candidates for the bright- and dark-end members might be.

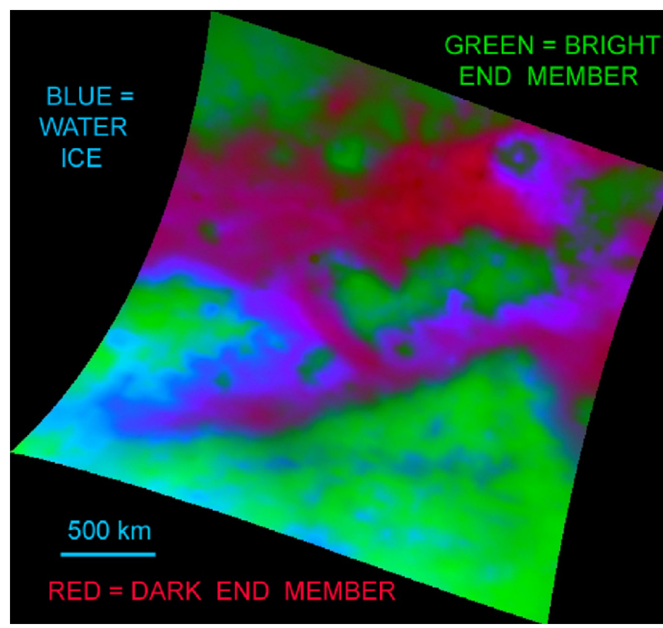

Fig. 6. Map of relative abundance of the three end members decomposed into the ternary coordinates for the cluster illustrated in Fig. 5. Image coordinates and projection identical to Fig. 3.

3. Correlation of VIMS dark brown unit with RADAR SAR dunes

The Cassini RADAR investigation has returned SAR image swaths that range in latitude from ~65°S to ~88°N and now cover >15% of the surface of Titan at resolutions down to ~350 m (Elachi et al., 2005; Lorenz et al., 2006; Stofan et al., 2007; Lunine et al., submitted). A number of these swaths have imaged the equatorial and mid-latitude regions. Lorenz et al. (2006) describe vast seas of sand dunes in parts of the equatorial-to-mid-latitude region imaged on Titan passes T_3 (February 15, 2005) and T_8 (October 28, 2005). These eolian units are characterized by long linear dune features that are interpreted to be longitudinal dunes formed by sand-sized (100–300 μm) saltating particles. Fig. 7 shows an example of these features where individual isolated dunes stand out against a radar-bright region imaged on pass T_3 in a north equatorial region. In SAR images the dunes are dark, having low RADAR backscatter. Where they occur in broad equatorial belts they are correlated with dark regions seen in optical images from the Cassini Imaging Science Subsystem (Porco et al., 2005).

Fig. 8 illustrates at a scale large enough to easily distinguish the dunes, the strong correlation between the

Please cite this article as: Soderblom, L.A., et al., Correlations between Cassini VIMS spectra and RADAR SAR images: Implications for Titan's surface composition and the character of the Huygens Probe Landing Site, Planet. Space Sci. (2007), doi:10.1016/j.pss.2007.04.014

VIMS dark brown units and dune fields discovered in SAR images. The 70-km diameter Sinlap impact crater is visible on the right edge of the left panels. The right views are of the Antilia Faculae feature (the roughly circular feature to the right of center) an 80-km diameter structure that could be an older degraded impact or volcanic crater. Fig. 9 extends the correlation between the SAR dunes and VIMS dark brown unit to the entire regions of joint coverage for the areas shown in Fig. 8. These observations clearly illustrate that the SAR dunes are strongly correlated—possibly uniquely—with the dark brown unit inferred as water ice poor. Subsequent VIMS observations of dunes from T_4 continue to support this correlation (Barnes et al., 2007).

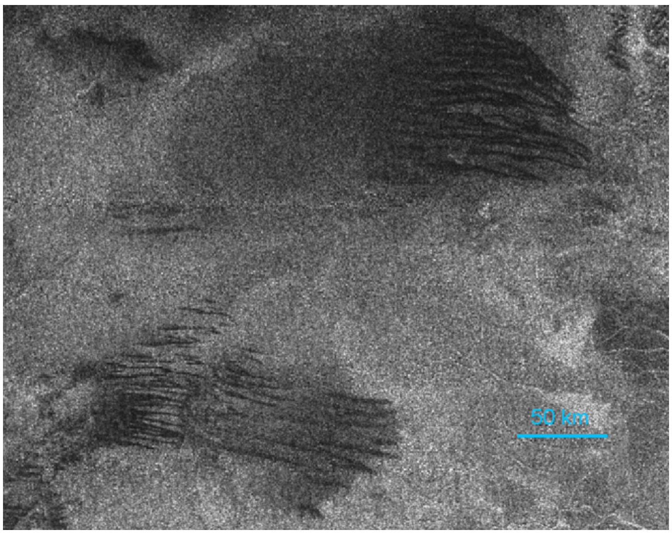

Fig. 7. Longitudinal dunes discovered in the Titan pass T_3 Cassini RADAR SAR swath. The area covered is ~250 km wide and is centered near 16°N, 93°W (projected in simple cylindrical).

4. RADAR-VIMS correlations in non-dune areas

Whereas the correlation between the VIMS dark brown units and the SAR dunes is quite evident, the correlations between the VIMS dark blue and bright units and the RADAR SAR units are elusive; in fact they exhibit no obvious correlation in Figs. 8 and 9. The area shown in Fig. 10 comprises largely VIMS bright and dark blue units where comparison with SAR gives some hint of correlation. The upper two panes cover an area ~300×1000 km in Omacatl Macula centered near 20°N45°W. Dunes are generally rare in this area although a patch of dunes, visible in the enlargement in the lower right panel (indicated by the blue arrow), illustrates that the correlation of the VIMS dark brown unit with RADAR SAR dunes holds for this area as well. The two lower left RADAR SAR insets (with

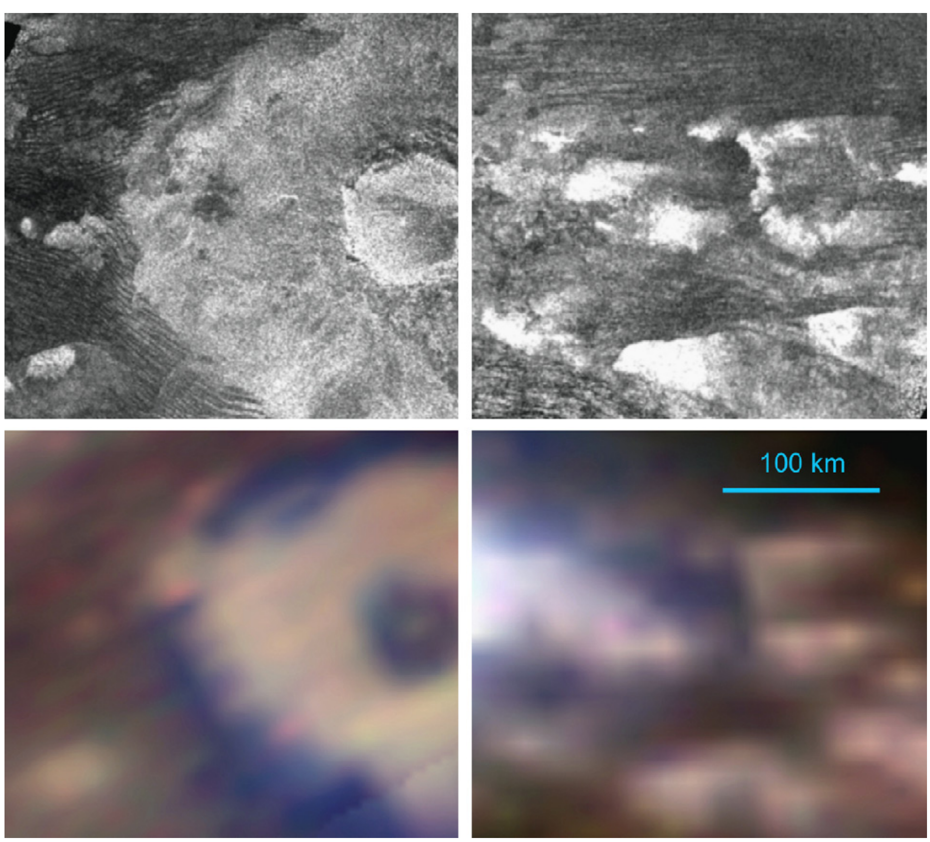

Fig. 8. Enlarged views of VIMS-RADAR correlations. The VIMS images (lower panels) employ the same spectral-band color composite as in Figs. 1 and 3. Projections are simple cylindrical. The left views (SAR from T_3; VIMS from T_5, center latitude/longitude ~11°N, 18°W) are of part of Sinlap crater (also visible in Fig. 3). The right views (SAR from T_8; VIMS from T_a, center latitude/longitude ~11°S, 191°W) are of the Antilia Faculae region (also seen in Fig. 1) approximately 150 km east of the Huygens landing site. Full views of these same data sets are shown in Fig. 9.

Please cite this article as: Soderblom, L.A., et al., Correlations between Cassini VIMS spectra and RADAR SAR images: Implications for Titan's surface composition and the character of the Huygens Probe Landing Site, Planet. Space Sci. (2007), doi:10.1016/j.pss.2007.04.014

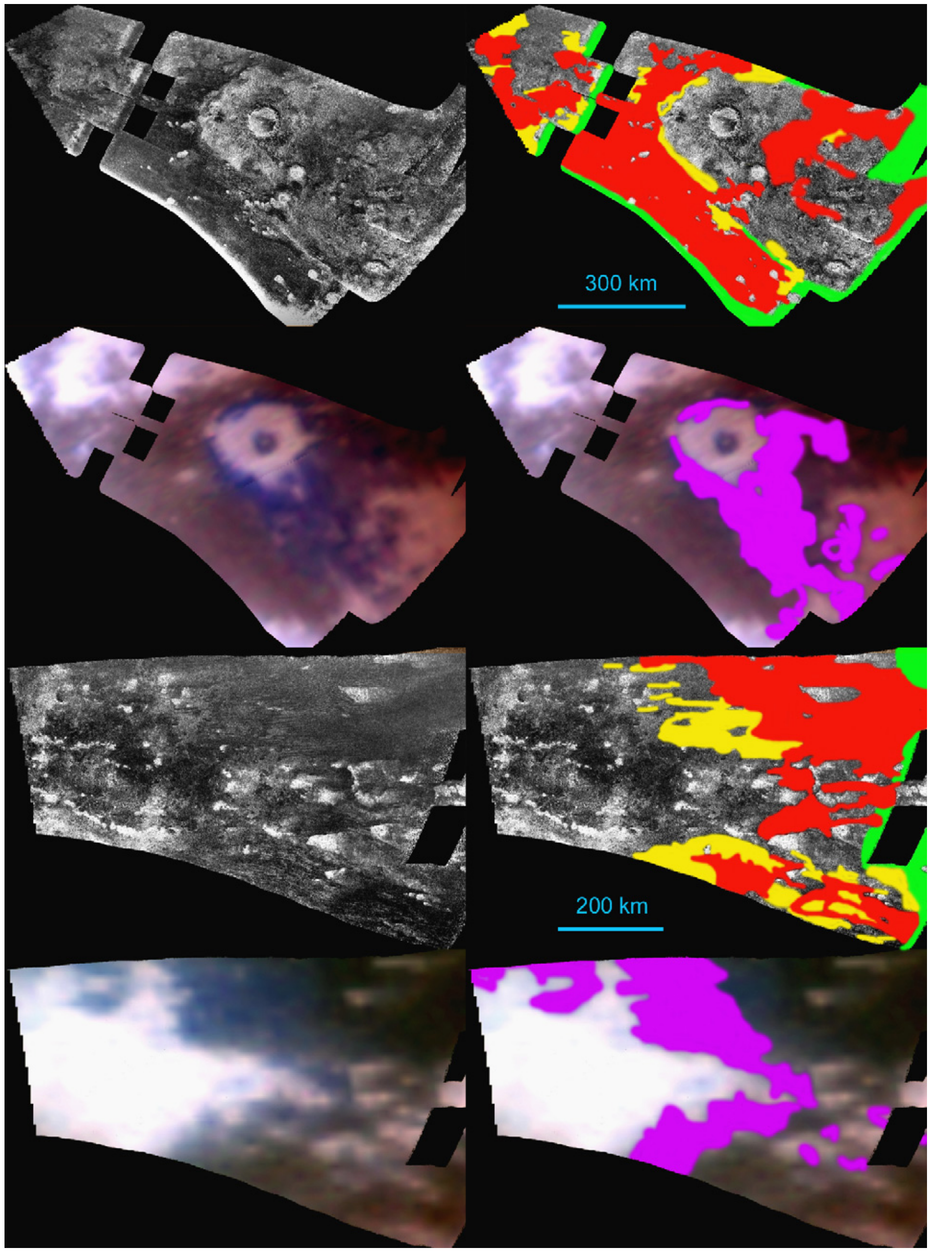

Fig. 9. VIMS-RADAR SAR correlation sketch maps. *Upper:* Sinlap region (also see Figs. 3 and 8): area shown is ~1140 km wide (center latitude/longitude ~8°N, 17°W). *Lower:* HLS region (also see Figs. 1 and 8): area shown is ~880 km wide (center latitude/longitude ~11°S, 194°W). The RADAR SAR units are mapped as follows: red = solid dune coverage, yellow = partial dune coverage, green = not mappable. Generalized sketch maps of the VIMS dark blue units are shown as magenta. Projections are simple cylindrical. Color composites use same spectral channels as Fig. 1.

green arrows) illustrate that in this region the dark blue units are often correlated with sinuous channel-like and flow features in the RADAR images, although both SAR-bright and SAR-dark cases are observed. Likewise the SAR-bright areas in the uppermost panel (red arrows), interpreted as rough hills, are correlated with both VIMS bright and VIMS dark blue units.

5. VIMS-RADAR correlations at the Huygens landing site

In Fig. 11, a DISR image mosaic is overlaid on the T_8 pass SAR swath and on the VIMS T_a color image composite. These are the same two VIMS and SAR data sets as shown in Figs. 1 and 9. The DISR mosaic comprises the highest-resolution HRI and MRI (High-Resolution Imager and Medium-Resolution Imager) images along with the two best SLI images (Side-Looking Imager) that view northward from ~45° above nadir to the horizon. These SLI images extend the coverage ~80 km north of the HLS and show east–west longitudinal dunes. As mentioned earlier, the positions of the SAR images are accurately known in the Titan inertial frame (error <10 km); the Huygens landing site is known with somewhat less accuracy in the inertial frame (probably ~20 km). From

Please cite this article as: Soderblom, L.A., et al., Correlations between Cassini VIMS spectra and RADAR SAR images: Implications for Titan's surface composition and the character of the Huygens Probe Landing Site, Planet. Space Sci. (2007), doi:10.1016/j.pss.2007.04.014

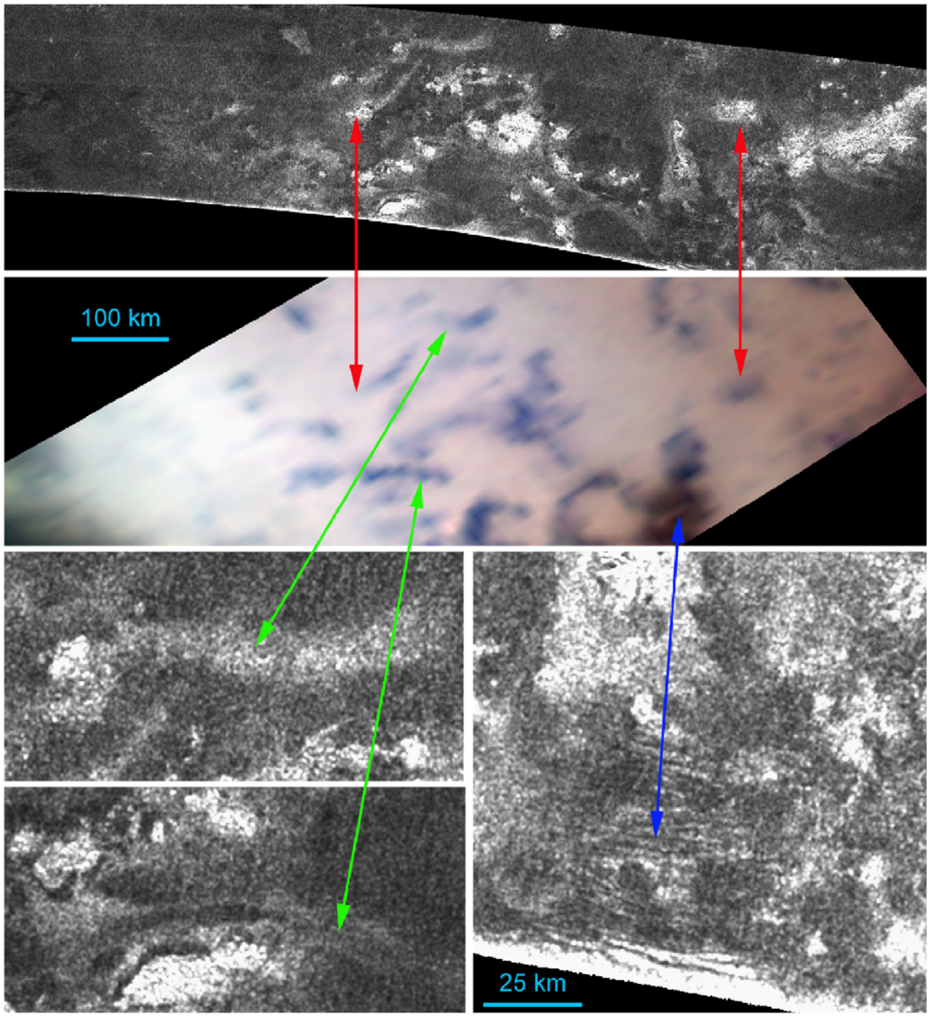

Fig. 10. Correlations between VIMS dark blue and bright units and RADAR SAR units. The top two panels are at the same scale with (center latitude/longitude ~19°N, 50°W; area ~950 km wide). Projections are simple cylindrical. *Top:* RADAR SAR image from central part of the T_3 swath *Middle:* VIMS color composite (same spectral channels as Fig. 1) from T_9. *Lower:* SAR insets enlarged by 4 × relative to the upper two panels. Blue arrow denotes a patch of dunes seen in RADAR that correlates with the VIMS dark brown unit. Red and green arrows denote RADAR-bright hills and flow-like features that sometimes correlate with VIMS dark blue units.

identification of two isolated longitudinal dunes in the SLI images, Lunine et al. (submitted) have identified the Huygens landing site in the T_8 SAR RADAR image (as annotated in Fig. 1). In addition to these two individual dunes that are ~30 km north of the landing site, another cluster of dunes slightly farther north are also seen in Fig. 11 and can also be correlated with parts of the RADAR SAR image as far as 60 km north of the landing site.

As shown in the bottom of Fig. 11, the region of the Huygens landing site is situated in a combination of VIMS bright and VIMS dark blue units. The inference is that the Huygens landing site, situated in the dark scoured plain (Tomasko et al., 2005), is in the VIMS dark blue unit that we interpret to be enriched in water ice relative to the brighter regions (or the dark brown dunes unit). The identification of water ice absorption at 1.54 μm in DISR near-infrared spectrum of the surface acquired after landing is consistent with the dark blue unit containing water ice. Tomasko et al. (2005) note that the absence of the weak water ice bands at 1.04 and 1.25 μm may be due to intimate mixing with dark hydrocarbon solids. Rodriguez et al. (2006) came to a similar conclusion showing the VIMS coverage of dark regions the landing site area is consistent with enrichment of water ice.

6. Discussion of compositional candidates

It is likely that the surface includes mechanical/chemical combinations of precipitates from upper atmospheric chemistry and chemistry combined with "geologic materials" derived from the crust and interior by fluvial/aeolian erosion, volcanism, and impacts. Water ice as one of the abundant compositional end members of Titan's surface materials is certainly reasonable based on global spectroscopy, the bulk density of Titan, and the abundant presence of water ice in the solar system. Interior models

Please cite this article as: Soderblom, L.A., et al., Correlations between Cassini VIMS spectra and RADAR SAR images: Implications for Titan's surface composition and the character of the Huygens Probe Landing Site, Planet. Space Sci. (2007), doi:10.1016/j.pss.2007.04.014

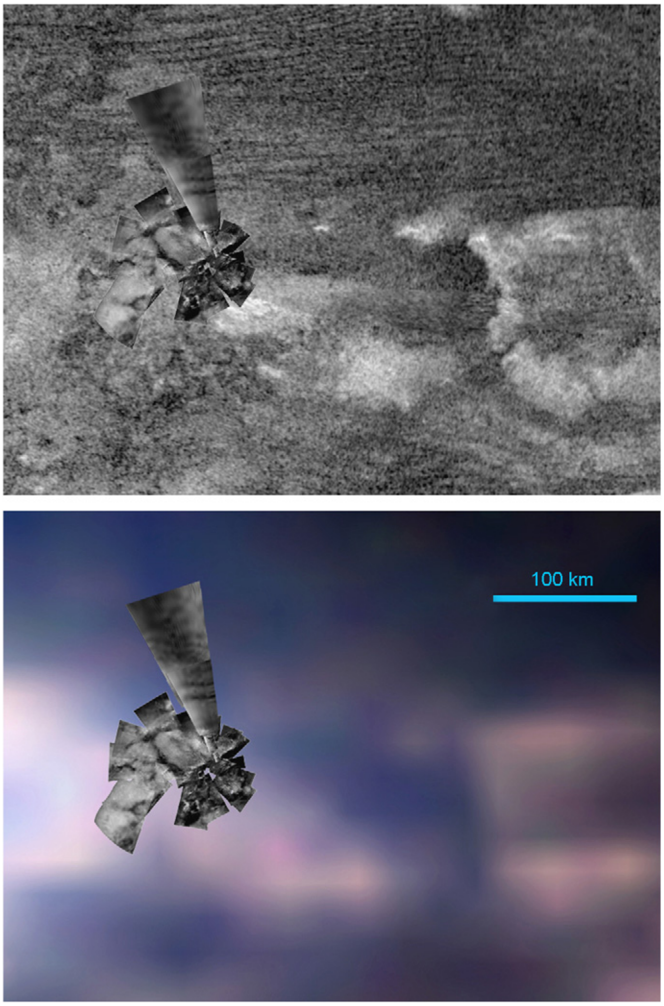

Fig. 11. Correlation of the DISR images with RADAR SAR (upper) and association with VIMS bright and dark blue surface units. Center latitude/longitude is ~10.4°S, 191.4°W; area is ~280 km wide. The Huygens landing site is ~30 km south of the nearest dunes. Projections are simple cylindrical; VIMS color composite as in Fig. 1.

suggest a mantle liquefied if ammonia is present, above and below which are layers of high pressure water ice and possibly methane clathrate, all surrounding a rocky core (Stevenson 1992; Lorenz and Lunine 2005; Tobie et al., 2006). Ammonia-water-hydrate volcanism could be profuse as this material has a density close to, and a much lower melting point (~176 K) than, pure water ice (Kargel et al., 1991, Yarger et al., 1993, Lorenz 1996). Ammonia-water slurries could erupt as viscous, gelatinous fluids depending on the proximity of their composition to the water-rich peritectic (Kargel et al., 1991). The Cassini RADAR has produced evidence of cryovolcanic flows and domes (Elachi et al., 2005; Lopes et al., 2007). The profuse eruption of water ice onto the surface represents one mechanism for exposing the primary crustal material to remote sensing spectrometers, against the tendency for burial by precipitating aerosols. However, fluvial or eolian transport of the aerosols might also uncover water ice "bedrock" as appears to happen on Mars. Our premise is that the VIMS dark blue units form a substrate that is enriched in water ice relative to either the VIMS dark brown units or most of the VIMS bright units, some of which show slight enrichment in the water ice end member (see Fig. 6). Water ice enrichment of the materials at the surface of the HLS and surrounding region is consistent with this view (Tomasko et al., 2005; Rodriguez et al., 2006).

The source of the bright end-member material is debated. Coustenis et al. (2001, 2005), Negrão et al. (2006, 2007), and Hirtzig et al. (2007) have proposed methane and ethane ices for these optically bright materials (and we could include propane). Although it is true that such ices have high reflectance in the 1.6 and 2.0 μm windows, matching those observed for Titan's equatorial bright regions, they are not stable as solids at Titan's equatorial surface temperature. Lindal et al. (1983) derived equatorial surface temperatures of 94.0 ± 0.7 K from Voyager Radio Occultation measurements whereas these ices all have melting points well below that (90.5, 89.7, and 85.3 K for methane, ethane, and propane, respectively). For these ices to be stable at the equatorial latitudes would require the bright terrains to be elevated at least 3–4 km above the mean surface of Titan (Lorenz and Lunine, 2005). Cassini RADAR altimetry measurements so far have shown no deviations of more than a few hundred meters from a hydrostatic figure (Lorenz et al., 2007). In addition the Huygens Atmospheric Structure Instrument measured an HLS surface temperature of 93.65 ± 0.25 K (Fulchignoni et al., 2005). The bright highland region 5 km north of the landing site is no more than 250 m above the adjacent plain (Tomasko et al., 2005; Soderblom et al., this issue). Thus, these alkanes would not be stable as solid "ices".

A plethora of solid organics are expected to form in the upper atmosphere from energetic chemistry (see McKay et al., 2001 for a review) and are likely to include acetylene, hydrogen cyanide, cyanoacetylene, cyanogen, and many other higher-order hydrocarbon compounds and nitriles. A broad suite of recent laboratory work has expanded the early studies of Khare et al. (1984) in synthesizing tholins, that could be representative of Titan aerosols, under various energy sources (including UV photolysis), varying composition, and over a range of pressure (Ramirez et al., 2002; Tran et al., 2003; Imanaka et al., 2004). These studies reveal many varieties with differing colors and albedos that could be forming in Titan's atmosphere. For example Imanaka et al. (2004, 2005) show that varying the pressure over that representative of altitudes where such materials should form in Titan's atmosphere, produces materials that have a broad range of absorptivity (varying by factors of several), including in the 1.3–2.0 μm spectral region studied here. This range of variance could explain the differences between the bright and dark water-poor end members in Figs. 5 and 6. We hypothesize that a reasonable candidate for the bright end member is a mantling deposit of bright aerosol dust that might include acetylene and other simple

Please cite this article as: Soderblom, L.A., et al., Correlations between Cassini VIMS spectra and RADAR SAR images: Implications for Titan's surface composition and the character of the Huygens Probe Landing Site, Planet. Space Sci. (2007), doi:10.1016/j.pss.2007.04.014

hydrocarbon solids whereas the dark water ice-poor end member of the dunes has a higher concentration of the more complex hydrocarbons and/or nitriles. It is possible that these hydrocarbons are intimately mixed with some water ice, spectrally masking the latter's presence. As noted by Lorenz et al. (2006) in order to facilitate eolian saltation, these dune materials must be very coarse grained (100–300 μm) compared to the aerosol fallout deposits. If they are derived from precipitating organic solids there must be some mechanism, whether mechanical and/or chemical, whereby the fine dust particles are built up into coarser saltating grains.

7. Summary

In conclusion, we propose a simple model for the composition of Titan's surface in which (1) the VIMS dark blue material comprises a dirty water ice substrate that is mantled in most places by the less water-rich bright and dark brown dune units; (2) the VIMS dark brown material that correlates with the RADAR SAR dunes consists of dark hydrocarbon and/or nitrile grains (perhaps mixed with some water ice) that are 100–300 μm in size, facilitating saltation (Lorenz et al., 2006); and (3) the VIMS bright regions are mantled by air-fall accumulations of bright aerosol hydrocarbon dust that is slightly enriched in water ice at some locales. We suggest the common occurrence of the dark blue unit as fringes on the margins of the bright units (as in Fig. 6) and the occasional correlation of dark blue units with flow and scour marks seen in the RADAR (as in Fig. 10) are consistent with a picture of bright mantles overlying a dark blue water-rich substrate. We further postulate that the bright mantling material is effectively transparent to RADAR. Thus the lack of correlation between RADAR images and the bright regions and their boundaries arises from this transparency. As a result the SAR images mostly show two units in the equatorial regions: vast thick deposits of the dark longitudinal dunes and features of the water ice-rich substrate, including roughness, fracture, porosity, and overall topography.

In this model the dark-floored dendritic channels pervasive in DISR images of the bright highlands a few km north of the HLS (Tomasko et al., 2005; Perron et al., 2006; Soderblom et al. this issue) are formed as the bright aerosol dust mantles are washed out of channel floors by liquid methane. It has been suggested that a slow, persistent methane drizzle continuously occurs (Tokano et al., 2006). It may be that the bright blankets of bright aerosol deposits are quite porous allowing gentle methane rain to permeate to the base of the bright mantle and to flow down-slope into the valleys where fluid collects with sufficient runoff rate to erode bright materials out of the dark-floored valleys. By contrast, the dark plain where Huygens landed may experience intermittent methane floods, not flowing from the highlands to the north but from sources to the west of the landing site as described in Soderblom et al. (this issue). These intermittent methane floods would then strip away mantling material, abrade and round water ice boulders, and exposing dark water ice-rich substrate.

Two alternatives could explain the segregation of the bright aerosol mantle and the dark brown hydrocarbon-rich dune materials. It is possible that some set of physical and/or chemical processes converts the bright fine-grained aerosol end-member into coarser dark end-member of hydrocarbon/nitrile grains that make up the dunes. As solid grains are built up they might become darker as scattering by fine particles is suppressed. Alternatively the source of the coarse dark dune materials may be totally different aerosol(s) than those making up the bright mantling materials-materials that have different optical properties, are generated at different altitudes and pressures by different processes, and are easily moved and coagulated into large saltating grains.

If the bright regions are simply coated by the fine-grained aerosol precipitating out of the atmosphere, erosive processes (wind, rain, and methane rivers and floods) must be continually etching the bright material off the darker surfaces exposing the VIMS dark-blue water-rich substrate as well as the VIMS dark brown dunes. As suggested by Smith et al. (1996) active processes must be renewing the contrast among surface regions. If the rate of deposition of bright material, for example from precipitating bright tholins and acetylene, is 0.001–0.01 μm/yr (Lara et al., 1994; Smith et al., 1996; McKay et al., 2001), the surface would be coated (to optical instruments) in hundreds-to-thousands of years unless cleansing processes are active. The dark dunes must be mobile on this short timescale to prevent the accumulation of bright coatings. Likewise fluvial/pluvial processes every few centuries or millennia must be cleansing the dark floors of the incised dendritic channels and dark scoured plains at the Huygens landing site that were both imaged by DISR.

Acknowledgments

This work was funded by the Cassini Project conducted for NASA by the Jet Propulsion Laboratory, California Institute of Technology. The authors wish to thank Athena Coustenis, Jeffery Johnson, Christopher McKay, Timothy Titus, and an unnamed reviewer for insightful and constructive criticism.

References

Barnes, J.W., Brown, R.H., Soderblom, L., Buratti, B.J., Sotin, C., Rodriguez, S., Le Mouèlic, S., Baines, K.H., Clark, R., Nicholson, P., 2007. Global-scale surface spectral variations on Titan seen from Cassini/VIMS. Icarus 186, 242–258.

Brown, R.H., Baines, K.H., Bellucci, G., Bibring, J.-P., Buratti, B.J., Capaccioni, F., Cerroni, P., Clark, R.N., Coradini, A., Cruikshank, D.P., Drossart, P., Formisano, V., Jaumann, R., Langevin, Y., Matson, D.L., McCord, T.B., Mennella, V., Miller, E., Nelson, R.M., Nicholson, D., Sicardy, B., Sotin, C., 2004. The Cassini Visual and Infrared Mapping Spectrometer (VIMS) investigation. Space Sci. Rev. 115 (1–4), 111–168.

Clark, R.N., Curchin, J., Brown, R.H., Cruikshank, D.P., Jaumann, R., Lunine, J., Hoefen, T., Baines, K.H., Buratti, B.J., Barnes, J., Nicholson, D., Stephan, K., 2006. Detection of widespread aromatic and aliphatic hydrocarbon deposits on Titan's surface observed by Cassini VIMS. In: AGU Fall Meeting, Abstract #P11A-03.

Coustenis, A., Lellouch, E., Maillard, J.P., McKay, C.P., 1995. Titan's surface, composition and variability from the near-infrared albedo. Icarus 118, 87–104.

Coustenis, A., Gendron, E., Lai, O., Véran, J.-P., Woillez, J., Combes, M., Vapillon, L., Fusco, T., Mugniez, L., Rannou, P., 2001. Images of Titan at 1.3 and 1.6 μm with adaptive optics at the CFHT. Icarus 154, 501–515.

Coustenis, A., Hirtzig, M., Gendron, E., Drossart, P., Lai, O., Combes, M., Negrão, A., 2005. Maps of Titan's surface from 1 to 2.5 μm. Icarus 177 (1), 89–105.

Coustenis, A., Negrão, A., Salama, A., Schulz, B., Lellouch, E., Rannou, P., Drossart, P., Encrenaz, T., Schmitt, B., Boudon, V., Nikitin, A., 2006. Titan's 3-micron spectral region from ISO high-resolution spectroscopy. Icarus 180, 176–185.

de Pater, I., Ádámkovics, M., Bouchez, A.H., Brown, M.E., Gibbard, S.G., Marchis, F., Roe, H.G., Schaller, E.L., Young, E., 2006. Titan imagery with Keck adaptive optics during and after probe entry. J. Geophys. Res. 111 (E7, E07S05), 1–16.

Elachi, C., Allison, M.D., Borgarelli, L., Encrenaz, P., Im, E., Janssen, M.A., Johnson, W.T.K., Kirk, R.L., Lorenz, R.D., Lunine, J.I., Muhleman, D.O., Ostro, S.J., Picardi, G., Posa, F., Rapley, C.G., Roth, L.E., Seu, R., Soderblom, L.A., Vetrella, S., Wall, S.D., Wood, C.A., Zebker, H.A., 2004. RADAR, the Cassini Titan RADAR Mapper. Space Sci. Rev. 115 (1–4), 71–110.

Elachi, C., Wall, S., Allison, M., Anderson, Y., Boehmer, R., Callahan, P., Encrenaz, P., Flamini, E., Franceschetti, G., Gim, Y., Hamilton, G., Hensley, S., Janssen, M., Johnson, W., Kelleher, K., Kirk, R., Lopes, R., Lorenz, R., Lunine, J., Muhleman, D., Ostro, S., Paganelli, F., Picardi, G., Posa, F., Roth, L., Seu, R., Shaffer, S., Soderblom, L., Stiles, B., Stofan, E., Vetrella, S., West, R., Wood, C., Wye, L., Zebker, H., 2005. First views of the surface of Titan from the Cassini RADAR. Science 308, 970–974.

Fulchignoni, M., Ferri, F., Angrilli, F., Ball, A.J., Bar-Nun, A., Barucci, M.A., Bettanini, C., Bianchini, G., Borucki, W., Colombatti, G., Coradini, M., Coustenis, A., Debei, S., Falkner, P., Fanti, G., Flamini, E., Gaborit, V., Grard, R., Hamelin, M., Harri, A.M., Hathi, B., Jernej, I., Leese, M.R., Lehto, A., Lion Stoppato, F., López-Moreno, J.J., Mäkinen, T., McDonnell, J.A.M., McKay, C.P., Molina-Cuberos, G., Neubauer, F.M., Pirronello, V., Rodrigo, R., Saggin, B., Schwingenschuh, K., Seiff, A., Simões, F., Svedhem, H., Tokano, T., Towner, M.C., Trautner, R., Withers, P., Zarnecki, J.C., 2005. In situ measurements of the physical characteristics of Titan's environment. Nature 438 (7069), 785–791.

Griffith, C.A., Owen, T., Geballe, T.R., Rayner, J., Rannou, P., 2003. Evidence for the exposure of water ice on Titan's surface. Science 300, 628–630.

Grundy, W.M., Schmitt, B., 1998. The temperature-dependent near-infrared absorption spectrum of hexagonal H_2O ice. J. Geophys. Res. 103 (E11), 25809–25822.

Hirtzig, M., Coustenis, A., Gendron, E., Drossart, P., Hartung, M., Negrão, A., Rannou, P., Combes, M., 2007. Titan, atmospheric and surface features as observed with Nasmyth Adaptive Optics System Near-Infrared Imager and Spectrograph at the time of the Huygens mission. J. Geophys. Res. 112 (E2, E02S91), 1–12.

Imanaka, H., Khare, B.N., Elsila, J.E., Bakes, E.L.O., McKay, C.P., Cruikshank, D.P., Sugita, S., Matsui, T., Zare, R.N., 2004. Laboratory experiments of Titan tholin formed in cold plasma at various pressures, implications for nitrogen-containing polycyclic aromatic compounds in Titan haze. Icarus 168, 344–366.

Imanaka, H., Khare, B.N., McKay, C.P., Cruikshank, D.P., 2005. Complex refractive indices of tholins produced from various initial gas mixtures and formation pressures: implications for Titan, the early Earth, and the outer solar system bodies. Bull. Am. Astron. Soc. 37, 772.

Kargel, J.S., Croft, S.K., Lunine, J.I., Lewis, J.S., 1991. Rheological properties of ammonia-water liquids and crystal-liquid slurries—planetological applications. Icarus 89, 93–112.

Karkoschka, E., 2006. 〈http://disr.lpl.arizona.edu〉.

Khare, B.N., Sagan, C., Arakawa, E.T., Suits, F., Callcott, T.A., Williams, M.W., 1984. Optical constants of organic tholins produced in a simulated Titanian atmosphere—from soft X-ray to microwave frequencies. Icarus 60, 127–137.

Lara, L.M., Lorenz, R.D., Rodrigo, R., 1994. Liquids and solids on the surface of Titan: results of a new photochemical model. Planet. Space Sci. 42, 5–14.

Lellouch, E., Schmitt, B., Coustenis, A., Cuby, J.-G., 2004. Titan's 5-μm light-curve. Icarus 168, 209–214.

Lindal, G.F., Wood, G.E., Hotz, H.B., Sweetnam, D.N., Eshleman, V.R., Tyler, G.L., 1983. The atmosphere of Titan—an analysis of the Voyager 1 radio occultation measurements. Icarus 53, 348–363.

Lopes, R.M.C., Mitchell, K.L., Stofan, E.R., Lunine, J.I., Lorenz, R., Paganelli, F., Kirk, R.L., Wood, C.A., Wall, S.D., Robshaw, L.E., Fortes, A.D., Neish, C.D., Radebaugh, J., Reffet, E., Ostro, S.J., Elachi, C., Allison, M.D., Anderson, Y., Boehmer, R., Boubin, G., Callahan, P., Encrenaz, P., Flamini, E., Francescetti, G., Gim, Y., Hamilton, G., Hensley, S., Janssen, M.A., Johnson, W.T.K., Kelleher, K., Muhleman, D.O., Ori, G., Orosei, R., Picardi, G., Posa, F., Roth, L.E., Seu, R., Shaffer, S., Soderblom, L.A., Stiles, B., Vetrella, S., West, R.D., Wye, L., Zebker, H.A., 2007. Cryovolcanic features on Titan's surface as revealed by the Cassini Titan Radar Mapper. Icarus 186, 395–412.

Lorenz, R.D., 1996. Pillow Lava on Titan, expectations and constraints on cryovolcanic processes. Planet. Space Sci. 44, 1021–1028.

Lorenz, R.D., Lunine, J.I., 2005. Titan's surface before Cassini. Planet. Space Sci. 53, 557–576.

Lorenz, R.D., Wall, S., Radebaugh, J., Boubin, G., Reffet, E., Janssen, M., Stofan, E., Lopes, R., Kirk, R., Elachi, C., Lunine, J., Mitchell, K., Paganelli, F., Soderblom, L., Wood, C., Wye, L., Zebker, H., Anderson, Y., Ostro, S., Allison, M., Boehmer, R., Callahan, P., Encrenaz, P., Ori, G.G., Francescetti, G., Gim, Y., Hamilton, G., Hensley, S., Johnson, W., Kelleher, K., Muhleman, D., Picardi, G., Posa, F., Roth, L., Seu, R., Shaffer, S., Stiles, B., Vetrella, S., Flamini, E., West, R., 2006. The Sand Seas of Titan: Cassini RADAR observations of longitudinal dunes. Science 312, 724–727.

Lorenz, R.D., Callahan, S., Gim, Y., Alberti, G., Flamini, E., Seu, R., Picardi, G., Orosei, R., Zebker, H., Lunine, J., Hamilton, G., Hensley, S., Johnson, W.T.K., Schaffer, S., Wall, S., West, R., Francescetti, G., 2007. Titan's shape, radius and landscape from Cassini Radar Altimetry. Lunar Planet. Sci. XXXVIII (LPI Cont. No. 1338), 1329.

Lunine, J.I., Elachi, C., Wall, S.D., Allison, M.D., Anderson, Y., Boehmer, R., Callahan, P., Encrenaz, P., Flamini, E., Franceschetti, G., Gim, Y., Hamilton, G., Hensley, S., Janssen, M.A., Johnson, W.T.K., Kelleher, K., Kirk, R.L., Lopes, R.M., Lorenz, R., Muhleman, D.O., Orosei1, R., Ostro, S.J., Paganelli, F., Paillou, P., Picardi, G., Posa, F., Radebaugh, J., Roth, L.E., Seu, R., Shaffer, S., Soderblom, L.A., Stiles, B., Stofan, E.R., Vetrella, S., West, R., Wood, C.A., Wye, L., Zebker, H., Alberti1, G., Karkoschka, E., Rizk, B., McFarlane, E., See, C., Kazeminejad, B. Cassini RADAR's third and fourth looks at Titan. Icarus, submitted for publication.

McCord, T.B., Hansen, G.B., Buratti, B.J., Clark, R.N., Cruikshank, D.P., D'Aversa, E., Griffith, C.A., Baines, E.K.H., Brown, R.H., Dalle Ore, C.M., Filacchione, G., Formisano, V., Hibbitts, C.A., Jaumann, R., Lunine, J.I., Nelson, R.M., Sotin, C., the Cassini VIMS Team, 2006. Composition of Titan's surface from Cassini VIMS. Planet. Space Sci. 54, 1524–1539.

McKay, C.P., Coustenis, A., Samuelson, R.E., Lemmon, M.T., Lorenz, R.D., Cabane, M., Rannou, P., Drossart, P., 2001. Physical properties of the organic aerosols and clouds on Titan. Planet. Space Sci. 49, 79–99.

Negrão, A., Coustenis, A., Lellouch, E., Maillard, J.-P., Rannou, P., Schmitt, B., McKay, C.P., Boudon, V., 2006. Titan's surface albedo variations over a Titan season from near-infrared CFHT/FTS spectra. Planet. Space Sci. 54, 1225–1246.

Negrão, A., Hirtzig, M., Coustenis, A., Gendron, E., Drossart, P., Rannou, P., Combes, M., Boudon, V., 2007. The 2-μm spectroscopy of Huygens probe landing site on Titan with very large Telescope/Nasmyth Adaptive Optics System Near-Infrared Imager and Spectrograph. J. Geophys. Res. 112 (E2, E02S92), 1–14.

Perron, J.T., Lamb, M.P., Koven, C.D., Fung, I.Y., Yager, E., Ádámkovics, M., 2006. Valley formation and methane precipitation rates on Titan. J. Geophys. Res. 111 (Issue E11, E11001), 1–14.

Porco, C.C., Baker, E., Barbara, J., Beurle, K., Brahic, A., Burns, J.A., Charnoz, S., Cooper, N., Dawson, D.D., Del Genio, A.D., Denk, T., Dones, L., Dyudina, U., Evans, M.W., Fussner, S., Giese, B., Grazier, K., Helfenstein, P., Ingersoll, A.P., Jacobson, R.A., Johnson, T.V., McEwen, A., Murray, C.D., Neukum, G., Owen, W.M., Perry, J., Roatsch, T., Spitale, J., Squyres, S., Thomas, P., Tiscareno, M., Turtle, E.P., Vasavada, A.R., Veverka, J., Wagner, R., West, R., 2005. Imaging of Titan from the Cassini spacecraft. Nature 434 (7030), 159–168.

Ramirez, S.I., Coll, P., da Silva, A., Navarro-González, R., Lafait, J., Raulin, F., 2002. Complex refractive index of Titan's aerosol analogues in the 200–900 nm domain. Icarus 156, 515–529.

Rodriguez, S., Le Mouélic, S., Sotin, C., Clénet, H., Clark, R.N., Buratti, B., Brown, R.H., McCord, T.B., Nicholson, D., Baines, K.H., the VIMS Science Team, 2006. Cassini/VIMS hyperspectral observations of the Huygens landing site on Titan. Planet. Space Sci. 54, 1510–1523.

Smith, P.H., Lemmon, M.T., Lorenz, R.D., Sromovsky, L.A., Caldwell, J.J., Allison, M.D., 1996. Titan's surface, revealed by HST imaging. Icarus 119, 336–349.

Soderblom, L.A., Tomasko, M.G., Archinal, B.A., Becker, T.L., Bushroe, W.L., Cook, D.A., Doose, L.R., Galuszka, D.M., Hare, T.M., Howington-Kraus, E., Karkoschka, E., Kirk, R.L., Lunine, J.I., McFarlane, E.A., Redding, B.L., Rizk, B., Rosiek, M.R., See, C., Smith, P.H., this issue. Topography and geomorphology of the huygens landing site on titan. Planet. Space Sci., doi:10.1016/j.pss.2007.04.015.

Stevenson, D.J., 1992. The interior of Titan. In: Proceedings of the Symposium on Titan, vol. ESA SP-338. ESA, Noordwijk, The Netherlands, pp. 29–33.

Stofan, E.R., Elachi, C., Lunine, J.I., Lorenz, R.D., Stiles, B., Mitchell, K.L., Ostro, S., Soderblom, L., Wood, C., Zebker, H., Wall, S., Janssen, M., Kirk, R., Lopes, R., Paganelli, F., Radebaugh, J., Wye, L., Anderson, Y., Allison, M., Boehmer, R., Callahan, P., Encrenaz, P., Flamini, E., Francescetti, G., Gim, Y., Hamilton, G., Hensley, S., Johnson, W.T.K., Kelleher, K., Muhleman, D., Paillou, P., Picardi, G., Posa, F., Roth, L., Seu, R., Shaffer, S., Vetrella, S., West, R., 2007. The lakes of Titan. Nature 445 (7123), 61–64.

Tokano, T., McKay, C.P., Neubauer, F.M., Atreya, S.K., Ferri, F., Fulchignoni, M., Niemann, H.B., 2006. Methane drizzle on Titan. Nature 442 (7101), 432–435.

Tobie, G., Lunine, J., Sotin, C., 2006. Episodic outgassing as the origin of atmospheric methane on Titan. Nature 440, 61–64.

Tomasko, M.G., Buchhauser, D., Bushroe, M., Dafoe, L.E., Doose, L.R., Eibl, A., Fellows, C., Farlane, E.M., Prout, G.M., Pringle, M.J., Rizk, B., See, C., Smith, H., Tsetsenekos, K., 2002. The Descent Imager/Spectral Radiometer (DISR) experiment on the Huygens Entry Probe of Titan. Space Sci. Rev. 104 (1), 469–551.

Tomasko, M.G., Archinal, B., Becker, T., Bézard, B., Bushroe, M., Combes, M., Cook, D., Coustenis, A., de Bergh, C., Dafoe, L.E., Doose, L., Douté, S., Eibl, A., Engel, S., Gliem, F., Grieger, B., Holso, K., Howington-Kraus, E., Karkoschka, E., Keller, H.U., Kirk, R., Kramm, R., Küppers, M., Lanagan, P., Lellouch, E., Lemmon, M., Lunine, J., McFarlane, E., Moores, J., Prout, G.M., Rizk, B., Rosiek, M., Rueffer, P., Schröder, S.E., Schmitt, B., See, C., Smith, P., Soderblom, L., Thomas, N., West, R., 2005. Rain, winds and haze during the Huygens probe's descent to Titan's surface. Nature 438 (7069), 765–778.

Tran, B.N., Joseph, J.C., Ferris, J.P., Persans, P.D., Chera, J.J., 2003. Simulation of Titan haze formation using a photochemical flow reactor—the optical constants of the polymer. Icarus 165, 379–390.

Yarger, J., Lunine, J.I., Burke, M., 1993. Calorimetric studies of the ammonia-water system with application to the outer solar system. J. Geophys. Res. 98 (E7), 13109–13117.